JAZF1: A Metabolic Regulator of Sensitivity to a Polyamine-Targeted Therapy

Spencer R. Rosario[1,2], Justine J. Jacobi[3], Mark D. Long[1], Hayley C. Affronti[3], Aryn M. Rowsam[3], and Dominic J. Smiraglia[3]

ABSTRACT

Identifying and leveraging unique points of metabolic dysregulation in different disease settings is vital for safe and effective incorporation of metabolism-targeted therapies in the clinic. In addition, it has been shown identification of master metabolic transcriptional regulators (MMTR) of individual metabolic pathways, and how they relate to the disease in question, may offer the key to understanding therapeutic response. In prostate cancer, we have previously demonstrated polyamine biosynthesis and the methionine cycle were targetable metabolic vulnerabilities. However, the MMTRs of these pathways, and how they affect treatment, have yet to be explored. We sought to characterize differential sensitivity of prostate cancer to polyamine- and methionine-targeted therapies by identifying novel MMTRs. We began by developing a gene signature from patient samples, which can predict response to metabolic therapy, and further uncovered a MMTR, JAZF1. We characterized the effects of *JAZF1* overexpression on prostate cancer cells, basally and in the context of treatment, by assessing mRNA levels, proliferation, colony formation capability, and key metabolic processes. Lastly, we confirmed the relevance of our findings in large publicly available cohorts of prostate cancer patient samples. We demonstrated differential sensitivity to polyamine and methionine therapies and identified JAZF1 as a MMTR of this response.

Implications: We have shown JAZF1 can alter sensitivity of cells and its expression can segregate patient populations into those that do, or do not highly express polyamine genes, leading to better prediction of response to a polyamine targeting therapy.

Introduction

Recently medical oncology has focused on exploiting tumor vulnerabilities as a means of treating patients. For example, chemotherapies target cancer's ability to proliferate (1, 2), targeted therapies (3) and tyrosine kinase inhibitors (4, 5) target single gene aberrations, and immunotherapies target deregulated immunosuppressive functions in tumors (6, 7). Metabolism is another potential vulnerability, as tumor cells alter normal cellular metabolism to support their high demand for energy and generation of biomass to support growth and proliferation (8, 9). This finding has led to a growing interest in identifying metabolic therapies as an alternative strategy for targeting cancer (10–13). However, a confounding issue with metabolic therapies is toxicity. Therefore, identifying metabolic vulnerabilities that are specific to a patient's tumor may reveal cancer therapies that can be administered with low toxicities.

To identify cancer-specific metabolic vulnerabilities, we have previously created a metabolic gene expression analysis pipeline that determines which of 114 metabolic pathways are most highly dysregulated in a tumor, as compared with matched normal tissues (14). This allows for the identification of metabolic pathways that are uniquely dysregulated in the tumor, offering cancer-specific targets that potentially reduce toxicity outside of the tumor. This approach identified the polyamine biosynthetic pathway, a pathway normally associated with the regulation of spermatic fluid components, as highly dysregulated and, more importantly, uniquely dysregulated in prostate cancer as compared with all tissues types (14).

We have previously shown that we can target polyamine biosynthesis using N^1, N^{11}-bis(ethyl)norspermine (BENSpm), which induces spermine/spermidine acetyltransferase (SSAT) and increases polyamine acetylation and export, and a methionine salvage pathway inhibitor, Methylthio-DADMe-Immucillin-A (MTDIA), which specifically inhibits Methylthioadenosine Phosphorylase (MTAP). This combination of BENSpm and MTDIA *in vitro*, *in vivo*, and *ex vivo* is highly effective in the treatment of prostate cancer (Supplementary Fig. S1; ref. 15), with limited toxicity. However, subsets of patient samples analyzed *ex vivo* do not respond (**Fig. 1**). Given this discrepancy, the development of a biomarker of response becomes necessary, especially for success in clinical trials (16). By applying bioinformatics approaches to studying the transcriptional reprogramming associated with the adaptive response to combination therapy, we can identify an innate transcriptional program associated with sensitivity or insensitivity to therapy. This analysis identified Juxtaposed Against Zinc Finger 1, JAZF1, as a commonly occurring master metabolic transcriptional regulator (MMTR), whose expression associates with response to polyamine-targeted therapies.

JAZF1 is a transcriptional repressor that has been shown to be highly associated with metabolic processes and with metabolism-related diseases such as diabetes (17–19) and fatty liver disease (20). Reduced expression of JAZF1 in diabetes leads to upregulation of glucose uptake, via stimulation of insulin receptor substrate and alpha serine/threonine protein kinase, and downregulation of gluconeogenesis via suppression of orphan nuclear receptor subfamily 2 group C member 2 (TR4) and glucose 6 phosphatase (17–19). In

[1]Department of Pharmacology and Therapeutics, Roswell Park Comprehensive Cancer Center, Buffalo, New York. [2]Department of Biostatistics and Bioinformatics, Roswell Park Comprehensive Cancer Center, Buffalo, New York. [3]Department of Cell Stress Biology, Roswell Park Comprehensive Cancer Center, Buffalo, New York.

Corresponding Author: Dominic J. Smiraglia, Roswell Park Cancer Institute, Elm & Carlton Streets, CGP L3–314, Buffalo, NY 14263. Phone: 716-845-1347; E-mail: Dominic.Smiraglia@roswellpark.org

Mol Cancer Res 2023;21:24–35

doi: 10.1158/1541-7786.MCR-22-0316

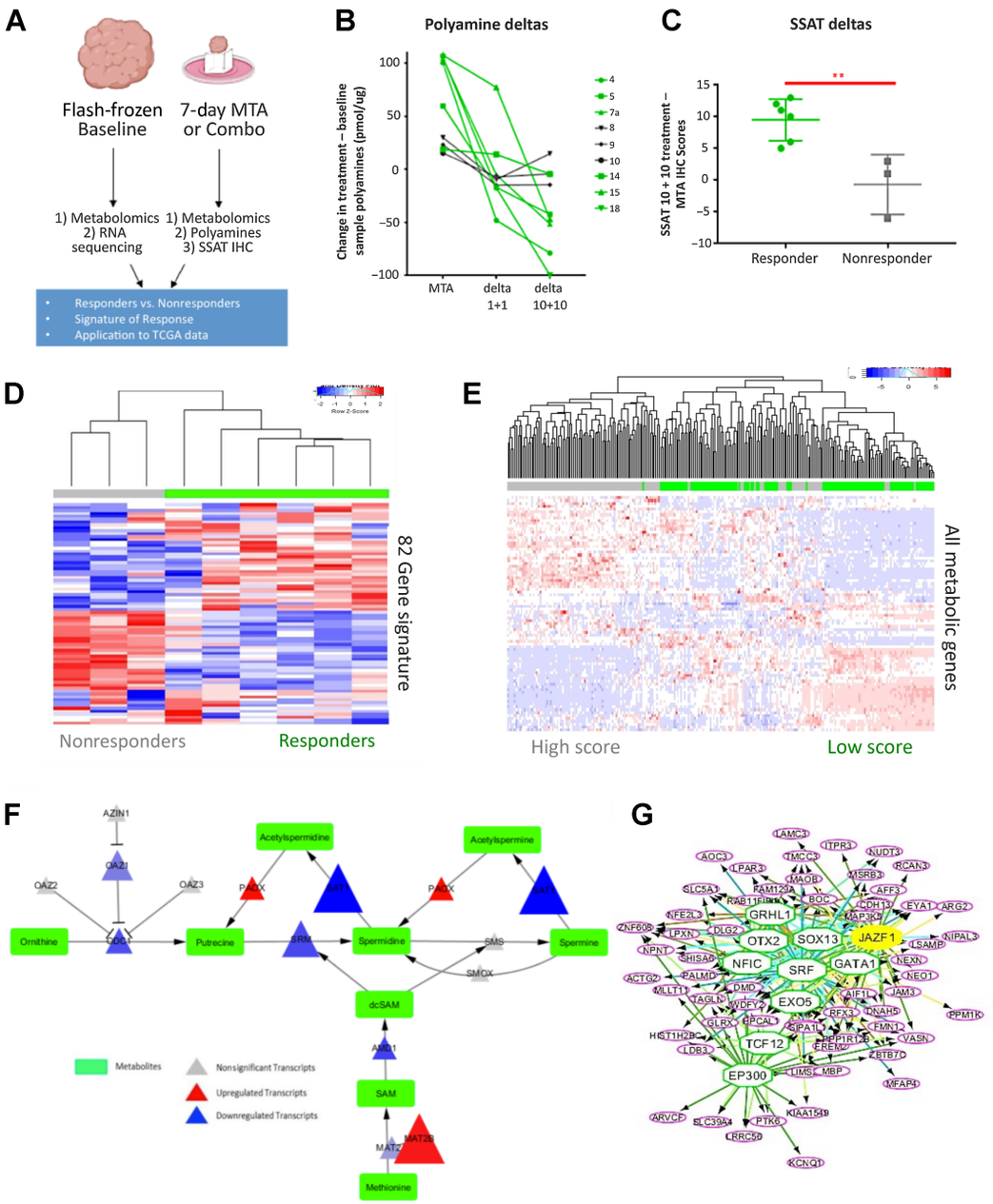

Figure 1.

Variable sensitivity to polyamine therapy in prostate cancer. **A,** Baseline patient tumors were sectioned and either flash frozen or treated on dental sponges for 7 days with vehicle control or two doses combination therapy (1 μmol/L BENSpm + 1 nmol/L MTDIA, or 10 μmol/L BENSpm + 10 nmol/L MTDIA). Baseline tumor (never treated) were used for RNA-seq to determine signatures of responders and nonresponders. **B,** Dose-dependent response to polyamine-targeted therapies as determined by measurement of polyamine levels revealed 6 responders (green) and 3 nonresponders (gray). **C,** IHC stained slides for SSAT indicated a change in index scores between vehicle control and 10 μmol/L BENSpm + 10 nmol/L MTDIA for responders and nonresponders. **D,** Unsupervised hierarchical clustering of samples based on DEGs show clear delineation between responders (green) and nonresponders (gray). **E,** Unsupervised hierarchical clustering of transcriptomic data from TCGA PRAD patients stratified into Q1 (nonresponders, gray) and Q4 (responders, green) based upon the 82-gene *ex vivo* signature scores across 1,843 metabolic genes. **F,** Comparison of TCGA predicted nonresponders to responders revealed nonresponders have lower levels of polyamine genes, compared with the responders (size of the triangle indicates FC, red = significantly upregulated, blue = significantly downregulated, gray = unchanged transcript). **G,** Master regulator enrichment of the *ex vivo* signature reveal potential transcriptional regulators of resistance to polyamine-targeted therapies.

fatty liver disease, JAZF1 regulates lipid droplet formation via stimulation of AMP-activated protein kinase (AMPK; 20). In hepatocytes, overexpression of JAZF1 attenuated expression of lipogenic genes including increased AMPK phosphorylation and decreased sterol regulatory element-binding protein 1c (21) expression, However, knockdown of JAZF1 reversed this phenotype, enhancing lipogenic gene expression (22, 23). The relationship between *JAZF1* expression and polyamine biosynthetic and methionine salvage metabolic pathways, have yet to be elucidated.

JAZF1 is commonly part of translocations in endometrial sarcoma where it forms fusion proteins with suppressor of zeste 12 homolog (SUZ12) and plant homeodomain (PHD) finger protein 1 (24, 25). These JAZF1 containing fusions are thought to disrupt transcription in a lineage-specific manner. However, the specific function of JAZF1 and SUZ12 genes in human malignant cells is still not known. Outside of endometrial sarcoma, increased JAZF1 expression has been associated with increased aggression of prostate cancer, which may be attributed to enhancement of JNK/SLUG signaling (26). In addition, several epidemiologic studies have demonstrated *JAZF1* single-nucleotide polymorphisms are associated with schizophrenia and decreased prostate cancer risk (27, 28).

Here, we identify JAZF1 as an important regulator of sensitivity to targeting polyamine metabolism and the methionine salvage pathway using *in vitro* and *ex vivo* prostate cancer systems and identify a gene signature associated with differential sensitivity. We further explore the molecular mechanism by which JAZF1 overexpression leads to decreased sensitivity to these targeted therapies. Finally, we use publicly available data from The Cancer Genome Atlas (TCGA; ref. 29) prostate adenocarcinoma (PRAD) cohort and the Taylor and colleagues (30) prostate cancer dataset, to confirm whether *JAZF1* levels correlate with polyamine pathway gene expression, associated with a predictive sensitivity or insensitivity to polyamine-targeted therapies on a larger patient cohort of data.

Materials and Methods

Ex vivo responder versus nonresponder stratification

Fresh tissue from radical prostatectomies performed on treatment naïve patients at Roswell Park Comprehensive Cancer Center (RP) was collected for *ex vivo* analysis as previously described (15). All of the tissue samples were collected under an Institutional Review Board (IRB)-approved protocol at Roswell Park Comprehensive Cancer Center. Specimens were collected after IRB-approved written consent from the patient was obtained at Roswell Park. Treatments and media were refreshed every 48 hours. Following 7 days of treatment, tissues were placed in 10% formalin and paraffin embedded for IHC or snap-frozen and kept at −80°C for polyamine quantitation.

Ultra-performance liquid chromatography analyses for polyamine and acetylated polyamine levels

Ultra-performance liquid chromatography (UPLC) analyses for polyamines were carried out similarly to previously described methods (31) with adjustments made to the flow rate, gradient, and column indicated below. Acetylated polyamines were extracted from media as previously described (15). A constant flow rate was held at 0.17 milliliters per minute, with a column temperature of 50°C and sample temperature of 5°C. Standards (Polyamines, acetylpolyamines, and BENSpm) were eluted using the same conditions and ranged in concentration from 1 to 100 μmol/L. Spike-ins of each standard confirmed the location of the peaks within the samples. Concentrations of polyamines were determined on the basis of standard curves and normalized to protein concentrations.

IHC

Freshly harvested tissues from the baseline and 7-day–treated *ex vivo* patient prostatectomy samples, were formalin-fixed and paraffin-embedded for immunohistologic analysis as previously described (32). Primary antibodies to Cleaved Caspase-3 from Cell Signaling Technology (CN: 9661), MTAP from Proteintech (CN: 11475–1- AP), and SSAT from Santa Cruz (CN: sc-67159) were used at dilutions of 1:200, 1:50, and 1:50, respectively.

Ex vivo tumor RNA extraction

Nine samples of human radical prostatectomy were snap-frozen upon extraction and RNA extracted using the TRIzol protocol. (Invitrogen, TFS CN: 15596018) Pellets were then resuspended in 30 to 50 μL of nuclease free water, and added ThermoFisher DNAse 1, RNAse-free buffer (TFS CN: EN0521) according to the instructions.

Ex vivo metabolomics

Samples were prepared and analyzed in the Roswell Park Comprehensive Cancer Center Bioanalytics, Metabolomics and Pharmacokinetics Shared Resource, using the MxP Quant 500 kit (Biocrates Life Sciences AG) in accordance with the user manual. Tumor samples were homogenized in a ratio of 1 mg of tissue to 3 μL of solvent (85% ethanol and 15% 0.01 mol/L phosphate buffer) using optimized setting on the Omni-Bead Ruptor 24 (Omni International). The homogenate was centrifuged to obtain a supernatant which was added to the plate (10 μL). Sample extract elution was performed with 5-mmol/L ammonium acetate in methanol and diluted with either water for the high pressure liquid chromatography (HPLC)-MS/MS analysis (1:1) or kit running solvent (Biocrates Life Sciences AG) for flow injection analysis–MS/MS (50:1), using a Sciex 5500 mass spectrometer. Data was processed using MetIDQ software (Biocrates Life Sciences AG), Limma (33) for differential metabolites and Metaboanalyst (34) for metabolite set enrichment analysis.

Ex vivo tumor RNA sequencing

RNA sequencing (RNA-seq) was performed by the Genomic Shared Resource at RP. Sequencing libraries were prepared with the TruSeq Stranded Total RNA Kit (Illumina Inc CN: RS-1222–2101), from 1 μg total RNA following the manufacturer's instructions. Libraries are purified and validated for appropriate size on a 2100 Bioanalyzer High Sensitivity DNA chip (Agilent Technologies, Inc.). Library pools are clustered and run on a HiSeq2500 rapid mode sequencer according to the manufacturer's recommended protocol (Illumina, Inc.). Raw reads passing the Illumina RTA quality filter are preprocessed using FASTQC for sequencing base quality control. Reads are mapped to the human reference genome (hg38) and RefSeq annotation database using Salmon. Salmon read outputs were then converted to transcript per million reads using the "TXImport" package in R (35).

Ex vivo drug sensitivity signature score

For differentially expressed gene (DEG) analysis, RNA-seq counts were processed to remove genes lacking expression in more than 80% of samples. Limma scale normalization, and voom transformation, were conducted in R on data from *ex vivo* responders and nonresponders were compared with generate DEG lists with an adjusted *P* value (adj.*P*.val) < 0.05, and a |log fold change (logFC)| > 0.58. This

analysis identified a set of 82 DEGs between responders and nonresponders. Weighted scores for each of these 82 genes were then constructed on the basis of:

$$-\log(\text{adj}.P.\text{val}) * \text{logFC}$$

Individual gene scores and overall sample scores revealed low scores associated with nonresponders and high scores associated with responders.

Ex vivo signature score applied to TCGA

RNA-Seq by expectation maximization (RSEM) gene levels were pulled for the 82 DEGs identified by comparing responders and nonresponders. Genes decreased in nonresponders were assigned a value of −1, and those increased in nonresponders were assigned a value of +1. Gene values for each of the TCGA prostate cancer samples were multiplied by −1/+1, respectively for each patient and summed. The 497 patient samples were broken into quartiles with the highest quartile having the highest scores, with the same expression patterns as responders, and those in the lowest quartile having the lowest scores, with expression patterns of the nonresponders. Upper and lower quartiles were then compared across all metabolic genes using the "Gplots" and "Heatmap.2" packages in R. Euclidian distances and hierarchal clustering were used to determine sample similarity.

DEG analysis

Gene expression data was analyzed using Bioconductor. RNA-seq RSEM counts were processed to remove genes lacking expression in more than 80% of samples. Scale normalization and moderated Student *t* tests were performed using empirical Bayes statistics in the "Limma" (33) package. The resulting *P* values were adjusted via Benjamini and Hochberg correction. DEGs were considered significant if the gene had an adj.*P*.val < 0.05, and a $|\text{logFC}| \geq 0.58$.

Polyamine network generation

Pathway maps were generated using Cytoscape (36), VizMapper functions. Pathway maps were based on existing KEGG pathways (37). Limma DEG analysis directed shading of genes within the pathway: red (positive FC, statistically significant), blue (negative FC, statistically significant), or gray (non-statistically significant). Analysis used DEGs from TCGA high versus TCGA low *ex vivo* scores and JAZF1 high versus normal and JAZF1 low versus normal.

Master regulator enrichment analysis

We used iRegulon (38), a Java add-on in Cytoscape, to identify MMTRs. This approach uses a large collection of transcription factor (TF) motifs (9,713 motifs for 1,191 TFs) and ChIP-seq tracks (1,120 tracks for 246 TFs). We imported lists of DEGs and enriched these lists for MMTRs by a ranking-and-recovery enrichment step, which was used to reconstruct networks of MMTRs.

Cell culture with drug

Androgen sensitive prostate cancer cell line LNCaP was purchased from the ATCC (Manassas, CA). The castration recurrent line LNCaP-C4–2 was gifted by Dr. James Mohler's laboratory (Roswell Park Comprehensive Cancer Center). The castration recurrent line CWR22-Rv1 was gifted by Dr. Barbara Foster's laboratory (Roswell Park Comprehensive Cancer Center). All cell lines were authenticated via short tandem repeat profiling. All cell lines were routinely tested for *Myoplasma* monthly using the MycoAlert Mycoplasma Detection Kit (Lonza), and were further tested prior to RNA-seq experiments. All cell lines, LNCaP, LNCaP-C4–2, and CWR22-Rv1 were maintained in RPMI1640 + 10% FBS + 1% Penicillin/Streptomycin. JAZF1-overexpressing cell lines were maintained in the same conditions as their parental counterparts. MTAP inhibitor MTDIA was synthesized by Dr. Jim Phillips at the Cleveland Clinic Taussig Cancer Institute. BENSpm was purchased via Synthesis Med Chem, Shanghai, China. Cells were cultured as previously described (1). LNCaP cells were allowed 24 hours for attachment prior to treatment. LNCaP-C4–2 and CWR22-RV1 cells underwent 48 hours of androgen depletion, RPMI1640 + 2% charcoal stripped FBS + 1% Penicillin/Streptomycin. After 24 and 48 hours respectively, cells were washed with PBS and refreshed with media containing vehicle control and 20 μmol/L methylthioadenosine (MTA), 1 μmol/L BENSpm, 1 nmol/L MTDIA, or the combination of 20 μmol/L MTA, 1 μmol/L BENSpm, and 1 nmol/L MTDIA for 8 days. Media and drug were refreshed every 48 hours, and cells were trypsinized and re-plated, as needed. Experiments were performed in biological triplicate.

Word cloud generation

Word clouds were generated as previously reported (39) using the 'WordCloud' Cytoscape plugin (40). Master regulators were determined for each of the individual DEG lists and compiled into one master list, where duplicates were not removed.

Volcano plots

Volcano plots were constructed as previously described (41) using the 'ggplot2' (42, 43) package in R. A Benjamini-Hochberg FDR-adjusted $P < 0.05$ was considered significant. All genes were highlighted according to significance and FC (gray, nonsignificant; green, significant by FC; blue, significant by adj.*P*.val; red, significant by FC and adj.*P*.val).

JAZF1 overexpression in cell lines

For stable expression of JAZF1 prostate cancer cell lines, were transduced with empty vector control (pLVP) or the Origene Lenti ORF clone of Human JAZF1 vector (OriGene CN: RC207288L1) lentiviral supernatants as previously described (44). Cells underwent Neomycin selection (Sigma-Aldrich CN: N6386) @200 μg/mL.

Proliferation assays

Cell lines were maintained and treated as previously described (Cell culture with drug). 100,000 cells/well were plated in a 6-well plate, on Day 0, and cells began treatment 24 or 72 hours later (in accordance with Cell culture with drug). Three wells of cells were trypsinized and collected (per cell line and treatment) every 2 days. Cells were then counted via trypan blue exclusion using the Beckman Coulter Vi-CELL BLU Cell Viability Analyzer (Beckman Coulter Life Sciences).

qRT-PCR

Five hundred nanogram of RNA was retrotranscribed using the RevertAid First Strand cDNA Synthesis Kit (TFS CN: K1621), following the assay directions. Samples were incubated in a PCR machine at 65°C for 5 minutes, then cooled on ice for ∼5 minutes. cDNA from tissue was diluted 1:30 and cell pellets were diluted 1:3. 1.5 μL of diluted cDNA was used for real-time RT-PCR, in duplicate, with the iTaq SYBR Green Supermix with ROX (Bio-Rad) on a StepOnePlusTM Real-time PCR System (Thermo Fisher Scientific), as directed. Primer sequences for GUSB, SSAT, PAOX, SMOX, MTAP, and JAZF1 can be found in the supplement (Supplementary Table S4).

Reactive oxygen species assays

Reactive oxygen species (ROS) were measured as previously described (45, 46) using the Thermo Fisher Amplex Red Kit (TFS CN# A22188). Plates were read at 545-nm excitation and 590-nm emission on a 96-well plate spectrophotometer. Fluorescence was normalized to protein obtained by Thermo Fisher Scientific Pierce BCA Protein Assay Kit (TFS CN: 23227) from remaining lysate. All samples quantified and are represented as relative to control untreated (vehicle) cells.

SSAT activity assays

SSAT activity was assayed as previously described (47, 48). Counts per minute were normalized to protein concentrations. All data is represented relative to control untreated (vehicle) cells.

Colony formation assays

This method was adapted from previously used methods (49, 50). Cell lines were plated in 6-well dishes at low density (1,000 cells/well) and attached overnight. CWR22-RV1 and LNCaP-C4–2 were reconditioned as previously described (Cell culture with drug). Day 0 pictures, prior to the addition of drug, were taken using an Olympus Microscope Camera and the Brightfield filter. Media with drug was refreshed every 48 hours, and pictures were taken every 5 days, until Day 25. Final pictures were taken on Day 25. At Day 25, media was removed, wells were carefully rinsed with cold PBS, and then fixed with 2 to 3 mL of a prepared crystal violet (CV)/Methanol mixture for an hour. CV was removed by pipette and rinsed by carefully dunking plates in a bucket filled with tap water. Plates were left to dry at room temperature (20°C). Pictures were taken of CV stained colonies. CV and colonies were dissolved in 0.1 mol/L sodium citrate with 50% ethanol, 200 μL was transferred to a 96-well plate and read on a spectrophotometer at an absorbance of 590 nm.

JAZF1 TCGA analysis

TCGA data was downloaded as previously described (*ex vivo* signature score). Expression level of *JAZF1* was quantitated in all 497 samples, and expression was divided into quartiles. The highest quartile was designated as high, resulting in 25% of patients regarded as high *JAZF1*, and the remaining 75% of patients regarded as low *JAZF1* (lower 3 quartiles). Scale normalization was conducted on this dataset using the Limma package in R. After Voom transformation, data from high *JAZF1* and low *JAZF1* expressers were compared with generate a DEG list, which was used for metabolic pathways analysis, polyamine network generation and correlation with expression of polyamine genes for each of these groups with *JAZF1* expression using the 'cor' and 'corplots' package in R.

Results

A subset of prostate cancer tumors are innately resistant to polyamine-targeted therapies

There is a concentrated effort focused on understanding the mechanism of acquired resistance to pharmacologic intervention. However, understanding innate sensitivity is equally important for assigning therapy to patients who are likely to respond. To better identify the optimal patient population for polyamine-targeted therapies (Supplementary Fig. S1), it is necessary to identify a signature of responders and nonresponders. To address this fundamental question, treatment-naïve radical prostatectomy samples were acquired to measure *ex vivo* response to BENSpm + MTDIA. Samples with > 40% carcinoma were sectioned for both baseline tissue with no culture, and vehicle control or two doses of combination therapy for 7 days in culture (**Fig. 1A**). These samples were then used to assess tissue polyamine levels and expression of SSAT, the target of BENSpm. BENSpm treatment stabilizes SSAT, greatly increasing its activity, which is expected to result in export of acetylated polyamines and therefore a decrease in tissue polyamines. Polyamine levels demonstrated a dose-dependent decrease in 6/9 (green) samples (**Fig. 1B**). The same 6/9 samples (green) also exhibited increased SSAT protein levels by IHC (Supplementary Fig. S2, representative image), comparing the high dose and vehicle control cultured samples (**Fig. 1C**). On the basis of these observations of response, we classified these cases as 6 responders and 3 nonresponders. The transcriptome of the treatment-naïve baseline samples for these 9 tumors were then sequenced to identify a signature associated with response to polyamine-targeted therapies based on the DEGs between responders (green) and nonresponders (gray). Unsupervised hierarchical clustering of the data clearly separated the 3 nonresponders from the 6 responders (**Fig. 1D**).

To understand the relevance of expression levels of these genes more broadly in the clinical scenario, we used the TCGA radical prostatectomy PRAD dataset. A gene signature score was generated on the basis of the 82 DEGs (Supplementary Table S1) identified in the 9 patient samples (6 responders and 3 nonresponders). These scores were then applied to the TCGA PRAD data to define quartiles of patients. We isolated patients that either existed within the upper quartile of scores (gray) indicative of a nonresponder score, and lowest quartile (green) indicative of a responder score (**Fig. 1E**). These two groups of patients were then clustered on the basis of expression levels of all 1,843 metabolic genes. As shown in **Fig. 1E**, patients in the upper or lower quartile based on the 82 gene signature score clearly clustered together based on expression of the 1,843 metabolic genes.

To identify which metabolic pathways distinguish the two groups of patients, we applied our previously developed metabolic pipeline (14). We found 10 metabolic pathways were significantly upregulated (9) or downregulated (1) between the nonresponder group and responders (Supplementary Table S2). The pathways identified in this analysis corresponded with the results of metabolomics analysis comparing tumor samples from nonresponders and responders treated with combination therapy (Supplementary Fig. S3), where the top metabolites differentially expressed were lipids, bile acids, and amino acids (Supplementary Fig. S3A). Using metabolite set enrichment analysis, differential metabolites enriched for amino acid metabolism, purine and pyrimidine metabolism, as well as lipid metabolic pathways, and not surprisingly polyamine biosynthesis (Supplementary Fig. S3B). When high scorers, predicted to be less sensitive to therapy (Q1) and low scorers, predicted to be more sensitive to therapy (Q4) were compared, and the polyamine biosynthetic pathway was mapped (**Fig. 1F**), most of the transcripts were downregulated in the predicted nonresponder group, as compared with the predicted responders. The combination therapy relies on promoting flux through polyamine biosynthesis (15), thus innate downregulation of this pathway at the gene expression level would inherently decrease flux, relieve stress, and reduce to response to therapy. The 82 genes that comprise the signature of response in patient samples treated *ex vivo* were enriched for MMTRs, and a network was created to highlight a more specific and easily detectable potential predictive biomarker to segregate responders and nonresponders (**Fig. 1G**).

In vitro RNA-seq data highlights *JAZF1* as a modulator of response to polyamine-targeted therapies

We reasoned that intersecting the MMTRs of the 82 genes differentially expressed between responders and nonresponders with

MMTRs that regulate any potential adaptive transcriptional response to the metabolic therapy would identify a prime candidate for further study into whether the MMTR predicts sensitivity. Previous studies have indicated BENSpm + MTDIA treatment leads to an initial slowing of proliferation by 4 days in LNCaP, (androgen-dependent), and LNCaP C4–2 (C4-2) cells (androgen-independent), with some cytotoxicity by 8 days and severe cytotoxicity by 12 days. This timeline is advanced by ∼4 days in the CWR22-RV1

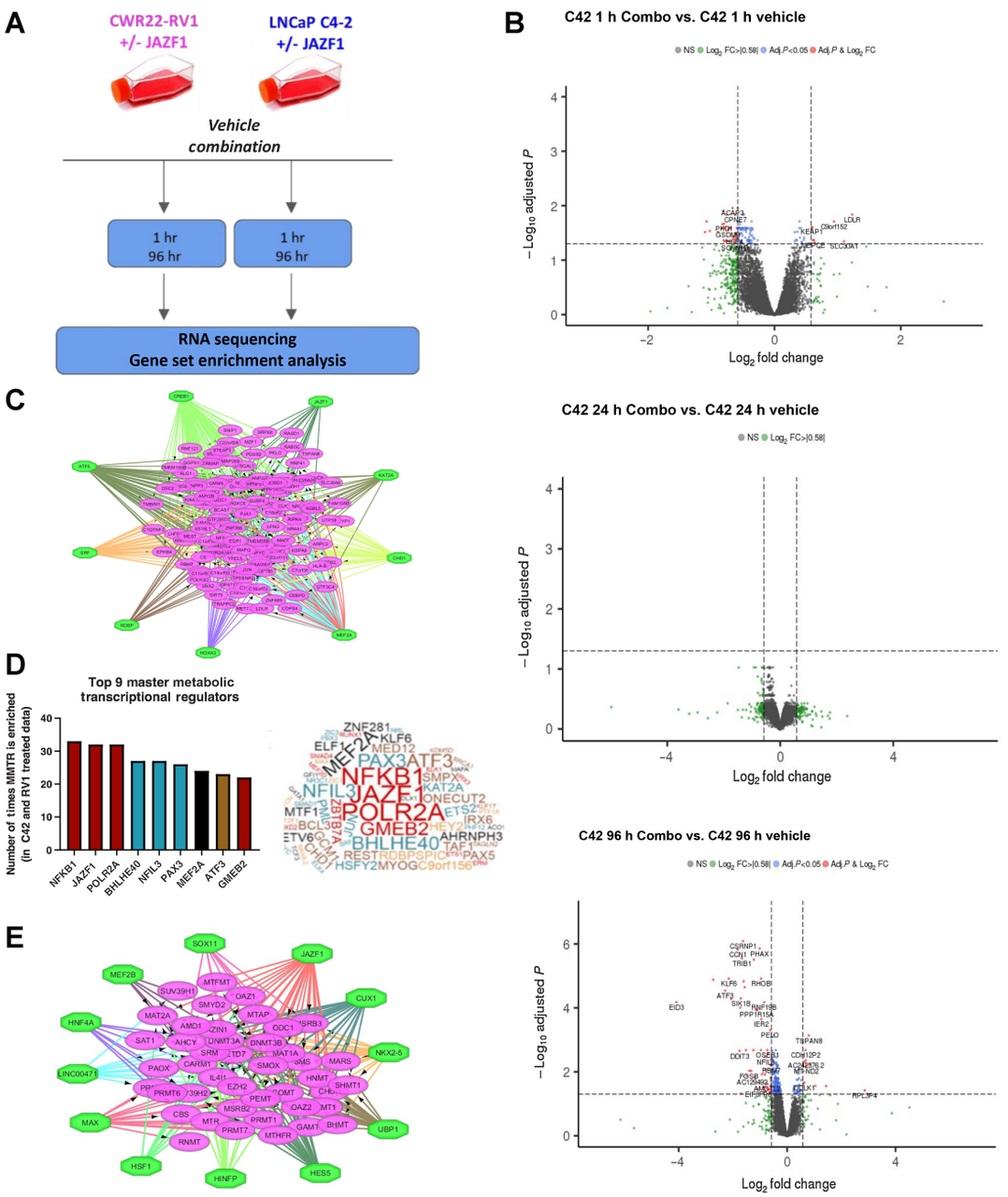

Figure 2.

MMTRs determine adaptation to polyamine-targeted therapies. **A,** CWR22-RV1 and LNCaP C4–2 cell lines were cultured with MTA (vehicle), single or combination therapy for varying time points. RNA was then collected and used for RNA-seq and then used for further MMTR analysis and gene set enrichment analysis. **B,** Volcano plots of RNA-seq data from LNCAP C4–2 cells comparing control-treated and combination-treated (BENSpm + MTDIA) at 1, 24, and 96 hours. (Significant genes are red). **C,** Example of MMTR analysis of the DEGs from the C4–2 96-hour combination versus vehicle treatment revealed master regulators for the time point. This was then overlapped with the master regulators of the other cell line, time points, and treatments to generate a (**D**) word cloud (right), where the size of the transcriptional regulator is indicative of how frequently it occurred, which is quantitated for the top 9 MMTRs (left). **E,** Further MMTR analysis of the polyamine and methionine cycles, the current targets of our drugs, similarly enriched for JAZF1 as a master regulator. *All experiments were a biological $n = 3$ and represent mean ± SD Significance calculated by Student t test, unless otherwise indicated.

(RV1), androgen-independent, cell line (15). Our goal was to understand adaptive mechanisms used to handle the metabolic stress being induced, rather than focus on what happens when the adaptive mechanisms ultimately fail at 8 to 12 days of treatment. Therefore, to delineate the adaptive mechanisms the cells use to maintain viability after metabolic dysregulation, the RV1 and C4–2 androgen-independent cell lines were treated with either vehicle (MTA), single agent (1 μmol/L BENSpm, or 1 nmol/L MTDIA), or combination therapy (**Fig. 2A**) for 1 hour, 24 hours, and 48/96 hours, respectively. At 48 hours, the biological effects on RV1 cell lines, is similar to 96 hours in C4–2 cell lines. RNA-seq was performed to identify the transcriptional reprogramming that occurs as a result of treatment. DEG analysis comparing control treatment to combination treatment indicated a cyclical pattern with initial transcriptional dysregulation (1 hour), a period of transcriptional restabilization (24 hours) and later transcriptional dysregulation, from which the cells do not recover (48/96 hours; C4–2: **Fig. 2B**, Rv1: Supplementary Fig. S4). Transcriptomic changes, as represented by DEGs over time (each cell line, each treatment, at each time point, as well as pooled DEGs and a separation of up and downregulated DEGs) were then independently enriched for MMTRs (**Fig. 2C**; Supplementary Fig. S5), and the results were pooled to determine the most commonly reoccurring MMTRs of the adaptive response (**Fig. 2D**). These results were then overlaid with the MMTRs of the polyamine biosynthetic and methionine pathways, which showed JAZF1 has binding motifs in key genes like *ODC1*, *MAT2A*, *PAOX*, and *SAT1* (**Fig. 2E**), as well as those associated with *ex vivo* sensitivity (**Fig. 1G**), to reveal JAZF1 as a common MMTR of the response to therapy and alteration of these two pathways.

JAZF1 overexpression results in conferred resistance to combination therapy

To determine how *JAZF1* expression relates to alterations in sensitivity to combination therapy, *JAZF1* was stably overexpressed in the androgen-dependent LNCaP, and the androgen-independent RV1 and C4–2 prostate cancer cell lines. While RV1 and C42 cell lines had higher levels of induced *JAZF1* as compared with their parental cell lines (500-fold), LNCaP had lower levels of induced *JAZF1* (5-fold) as compared with their parental cell lines. However, this discrepancy did not affect the phenotype that results from *JAZF1* overexpression. *JAZF1* overexpression significantly increased the basal growth rate after 8 days in all three cell lines (**Fig. 3A**, left). Moreover, *JAZF1* overexpression decreased sensitivity to combination therapy after 8 days (**Fig. 3A**, right). Overexpression of *JAZF1* in all three cell lines also resulted in decreased mRNA expression of key polyamine metabolism genes, including *SMOX* and *PAOX* (**Fig. 3B**), which mediate the generation of the ROS H_2O_2, which has been shown to contribute to the cytotoxic effects of this combination therapy (15). In addition, overexpression of *JAZF1* resulted in decreased mRNA expression of *SAT1* and *MTAP* (**Fig. 3B**), the targets of BENSpm and MTDIA, respectively. Overexpression of *JAZF1* resulted in decreased basal levels of ROS (H_2O_2) for all three cell lines, (**Fig. 3C**), and decreased ROS induction with both single-agent and combination therapy. Furthermore, SSAT enzymatic activity was decreased at baseline in vehicle control *JAZF1* overexpressing lines, and the level of induction by combination therapy was significantly reduced (**Fig. 3D**).

Given that *JAZF1* overexpression resulted in reduced activation of polyamine catabolism in response to therapy (lower ROS induction, lower expression of catabolic enzymes, reduced SSAT activity), we asked how internal polyamine pools and secreted acetylated polyamines were affected. As expected, both BENSpm and combination treatment led to increases in the spermidine:spermine ratio in both LNCaP and C4–2 cells. However, this distortion of the ratio in response to therapy is abrogated with *JAZF1* overexpression. (**Fig. 3E**). These findings are consistent with reduced activation of SSAT activity resulting in reduced flux through polyamine catabolism. Finally, *JAZF1* overexpression abrogated the cytotoxic effects of the combination therapy, as exemplified by the ability of *JAZF1* overexpressing cells, but not parental control cells, to form colonies after 15 days of combination therapy, as shown by microscopy (**Fig. 3F**; Supplementary Fig. S6), and quantitated cell density by CV staining at day 25 (**Fig. 3G**). Together, this provides a molecular mechanism that suggests *JAZF1* overexpression enhances proliferation and colony formation under combination therapy by decreasing key polyamine transcript levels, key polyamine enzyme activity, and ROS levels, and preventing the depletion of polyamine pools in the cells, all resulting in decreased sensitivity to treatment with BENSpm and MTDIA.

JAZF1 induces global transcriptional reprogramming and predicts patient stratification

To understand the full scope of transcriptional and metabolic changes associated with JAZF1, CWR22-RV1, and LNCaP-C4–2 parental and *JAZF1*-overexpressing cell lines underwent RNA-seq after treatment for 1 hour and 96 hours with either vehicle and combination (**Fig. 4A**). Cluster analysis of the expression of all 1,843 metabolic genes indicated that the presence of *JAZF1* overexpression drove the transcriptional differences between all samples, regardless of length of treatment or treatment itself (**Fig. 4B**). Overexpression of *JAZF1* resulted in global metabolic reprogramming, especially in key metabolic pathways such as oxidative phosphorylation and lipid-using pathways (**Fig. 4C**), which is a known role of JAZF1 (37). Further, many of these pathways corresponded with metabolite set enrichment analysis (Supplementary Fig. S3), of non-responder and responder tumor samples, which highlighted nicotinamide metabolism and lipid metabolic pathways. We next asked if high-level expression of *JAZF1* in prostate cancer patient samples also led to altered metabolic gene expression. When the TCGA PRAD cohort was grouped by quartiles of *JAZF1* expression and cluster analysis was performed on all metabolic genes, we observed strong clustering, via Euclidian distances, of the highest *JAZF1* expressing quartile (Q1; **Fig. 4D**). The polyamine biosynthetic pathway dysregulation, which we have previously demonstrated is highly upregulated in the total TCGA PRAD cohort (29), was instead strongly downregulated in patients who express high levels of *JAZF1* (**Fig. 4E**), especially genes involved in polyamine catabolism. Moreover, we found that most genes within the pathway were negatively correlated with *JAZF1* expression (**Fig. 4F**). In addition, overlaying the *JAZF1* status (high or low) with the 82 gene *ex vivo* score, resulted in substantial overlap between *JAZF1* increased expression and patients predicted to be resistant to therapy in the TCGA PRAD cohort (**Fig. 5A**). Further, there was statistically significant overlap between the increased *ex vivo* scores and increased *JAZF1* expression (**Fig. 5B**), indicating many of the patients with high *JAZF1*, do in fact have high *ex vivo* resistant scores. The positive correlation between *JAZF1* and *ex vivo* scores further extends to metastatic data (48), although, this is just a trend ($P = 0.06$; **Fig. 5C**). These findings strongly suggest that CaP patients with high levels of *JAZF1* have much lower flux through the polyamine pathway and would not be likely to respond as well to therapies aimed at activating polyamine catabolism, rendering them less sensitive. However, we also found metastatic samples

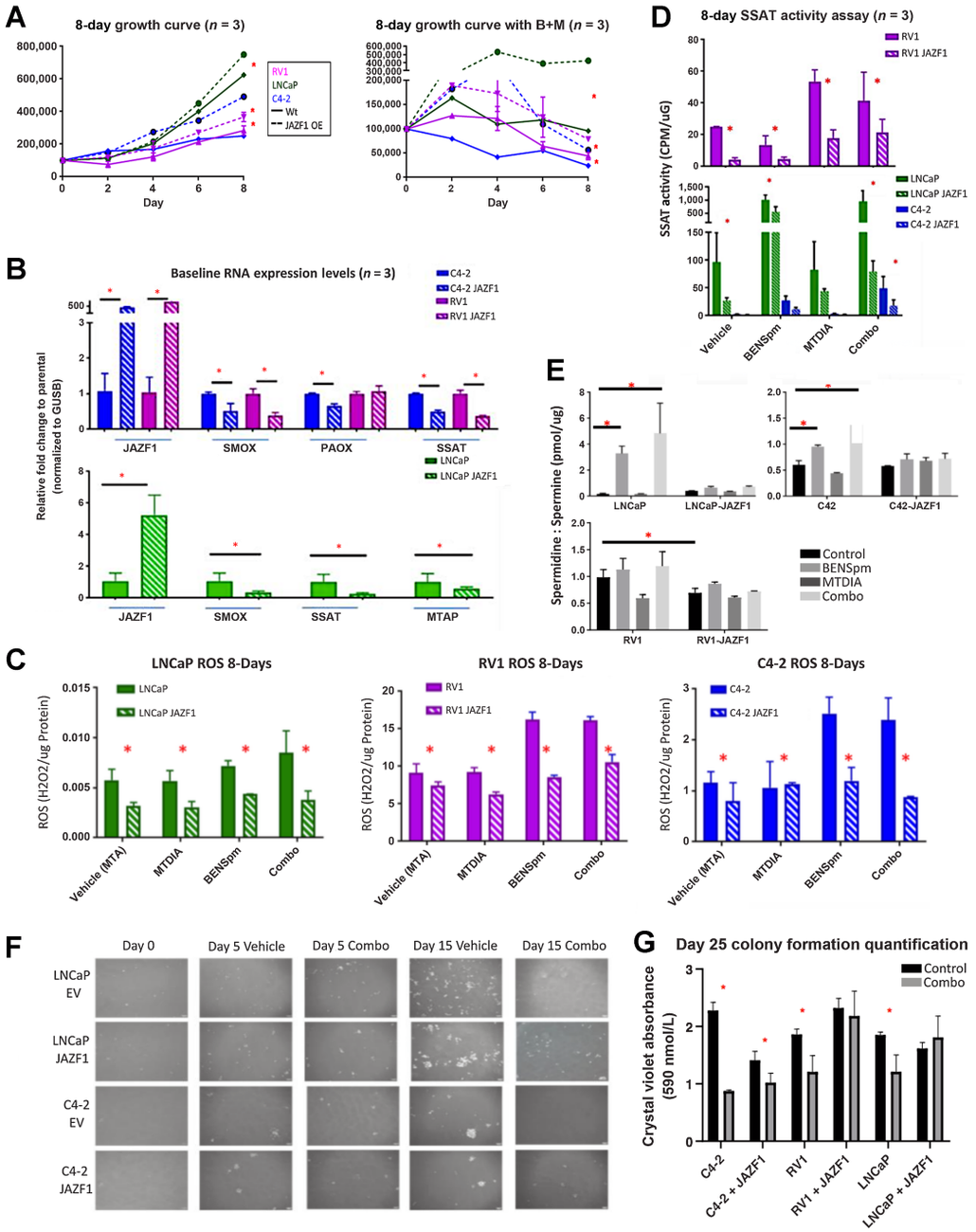

Figure 3.

JAZF1 overexpression confers resistance to polyamine-targeted therapies. **A,** JAZF1 overexpression leads to increased growth over 8 days for androgen sensitive (LNCaP) and insensitive (C4–2 and RV1) cell lines without (left) and with (right) combination therapy. **B,** Overexpression of *JAZF1* resulted in alterations of genes associated with response to treatment such as decreases n SSAT (target of BENSpm) and SMOX and PAOX (ROS producers) in both androgen-independent (blue and purple, top) and dependent (green, bottom) cell lines. **C,** Basal levels of ROS and ROS induction with treatment are decreased with *JAZF1* overexpression as compared with parental controls in both LNCaP C4–2 (blue, top) and LNCaP (green, bottom) cell lines (**D**) Both basal and combination treated SSAT activity is reduced across all cell lines with *JAZF1* overexpression as compared with parental controls. **E,** UPLC analysis of intracellular spermine and spermidine pools after 8 days of treatment indicates that the BENSPm and combination therapy induced distortion of the spermidine/spermine ratio abrogated with *JAZF1* overexpression. **F,** Representative images of colony formation with combination therapy in the parental cell lines (−JAZF1) and *JAZF1* overexpression (+JAZF1) cell lines, quantitated by CV. **G,** CV quantification at day 25 of the colony formation assay comparing the ratio of absorbance present in the combination/vehicle treated groups for each of the parental and *JAZF1* overexpressing cell lines, multiple *t* tests were performed to assess significance in the ratio between parental controls and the *JAZF1* overexpressing cell lines. *All experiments were a biological $n = 3$ and represent mean ± SD Significance calculated by Student *t* test, unless otherwise indicated.

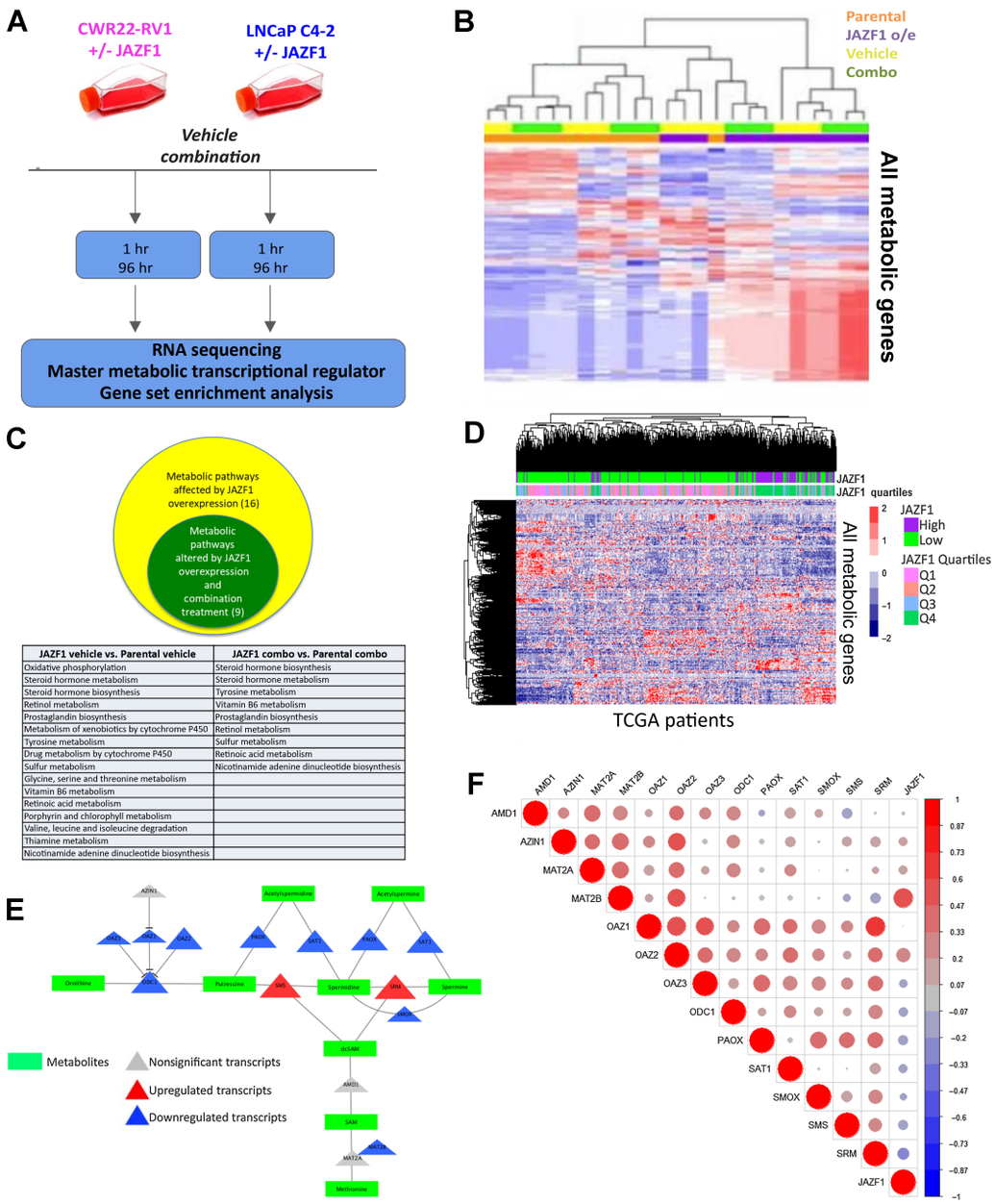

Figure 4.

JAZF1 overexpression reveals altered metabolism and predicts differential polyamine metabolism in TCGA Data. **A,** CWR22-RV1 and LNCaP-C42 parental cell lines and those overexpressing *JAZF1* were treated with vehicle control or combination therapy for 1 hour and 96 hours to assess the downstream transcriptional changes cells occur when *JAZF1* levels are high prior to and during polyamine-targeted therapy. **B,** Unsupervised hierarchical clustering on 1,843 metabolic genes demonstrating distinction between the RV1 parental (purple) and *JAZF1* (orange) overexpressing cell lines treated with vehicle (yellow) or combination (green) treatment or time points. **C,** Metabolic pipeline analysis revealed 16 metabolic pathways commonly altered (yellow) as a result of *JAZF1* overexpression, and 9 metabolic pathways (green) that remained altered with combination therapy, all of which were a subset of the 16 originally altered pathways. **D,** *JAZF1* high (purple) and low (green) patients are well segregated on the basis of the global expression of 1,843 metabolic genes. Quartiles also tend to closely follow high versus low designation (**E**) *JAZF1* high patients, overall, have lower expression of transcripts within the polyamine biosynthetic pathway, indicating they may not be primed for response to polyamine-targeted therapies. **F,** Correlation matrix between *JAZF1* expression levels in TCGA PRAD and polyamine metabolism genes. Node size, −log *P* value; red, positive correlations; blue, negative correlations.

(Supplementary Fig. S7) show altered polyamine transcripts that may be associated with vulnerability to polyamine-targeted therapies, we show that metastatic samples have less *JAZF1* (Supplementary Fig. S7A) but maintain the same negative correlation with polyamine-targeted genes (Supplementary Fig. S7B), and similar decreased expression of *ex vivo* resistance scores, predicting for increased sensitivity to polyamine intervention (Supplementary Fig. S7C).

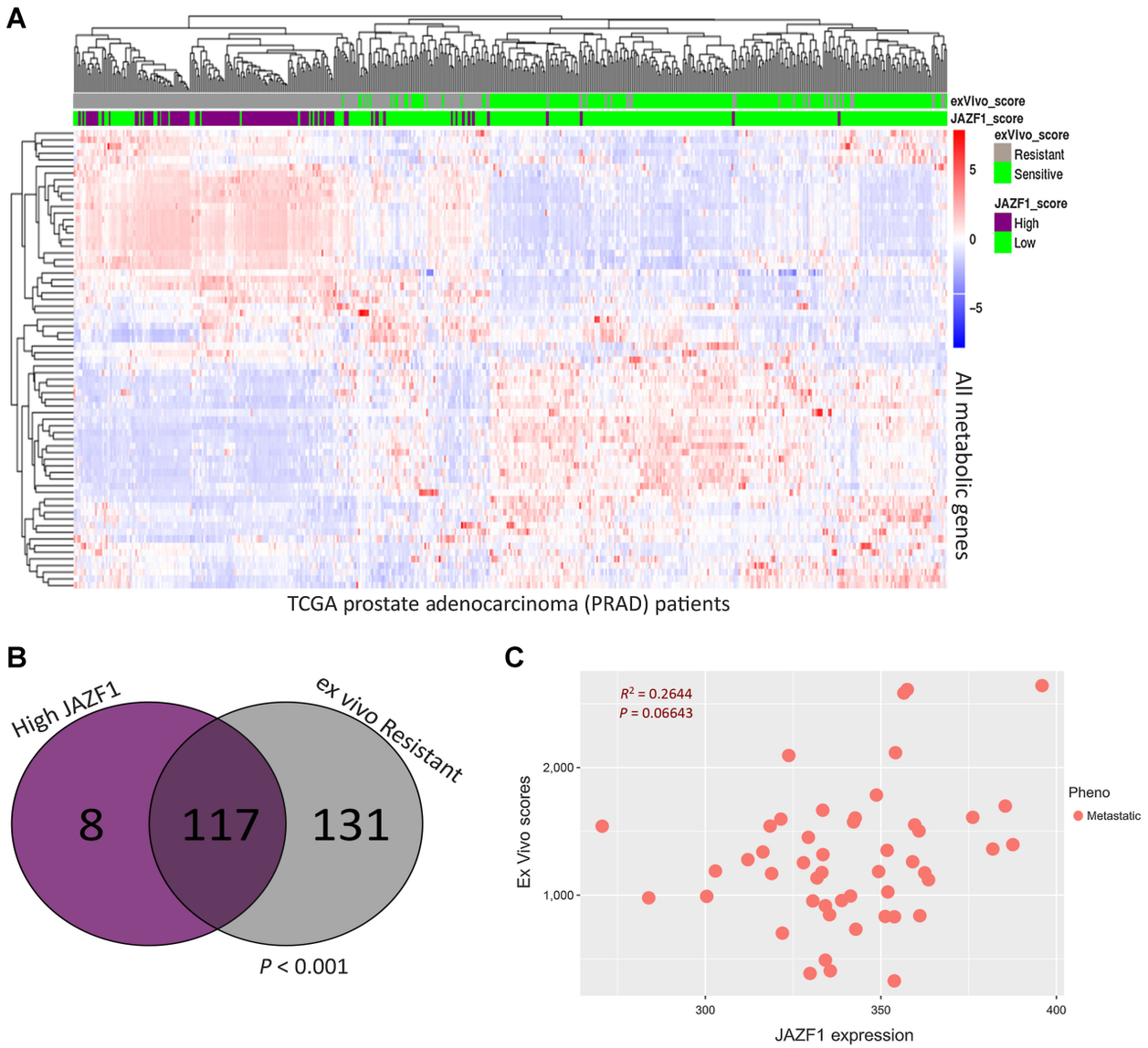

Figure 5.

Increased *JAZF1* corresponds with decreased predicted sensitivity to combination therapy. **A,** Unsupervised hierarchical clustering of transcriptomic data from TCGA PRAD patients stratified into JAZF1 expression high, top 25% (purple) and low, lower 75% (green) and *ex vivo* score predicted resistant, top 50% (gray) and predicted sensitive, lower 50% (green) based upon the 82-gene *ex vivo* signature genes. **B,** Venn diagram demonstrates a significant overlap of the patients with increased levels of *JAZF1* (purple) and predicted resistance to polyamine therapies by *ex vivo* score (gray). Significance determined by hypergeometric test. **C,** *JAZF1* and *ex vivo* prediction scores were positively correlated in the metastatic samples of the Taylor and colleagues dataset.

Discussion

The studies presented here demonstrate the utility of identifying and manipulating MMTRs as a means to identify optimal patient populations for metabolic based therapy. The approach successfully profiled MMTRs of both therapeutic response in *ex vivo* treated samples and adaptive response in multiple cell lines treated with combination therapy, both of which enriched for the MMTR, JAZF1. Further, we demonstrated the expression level *JAZF1* was correlated with metabolic reprogramming in patient prostatectomy samples from the larger TCGA cohort. Further, metabolic changes were consistent with changes that occur with *JAZF1* overexpression in prostate cancer cell lines.

JAZF1 has a demonstrated ability to affect the growth of these cells with and without polyamine-targeted therapies present in the cell culture environments and does so by targeting the major mechanisms of action of the polyamine-targeted therapies. By reducing the amount of SSAT present in the cells, as well as the ability to induce its enzymatic activity, there is an overall reduction in the amount of acetylated polyamines present in the system. In addition, the basal reduction in ROS levels, which is the major

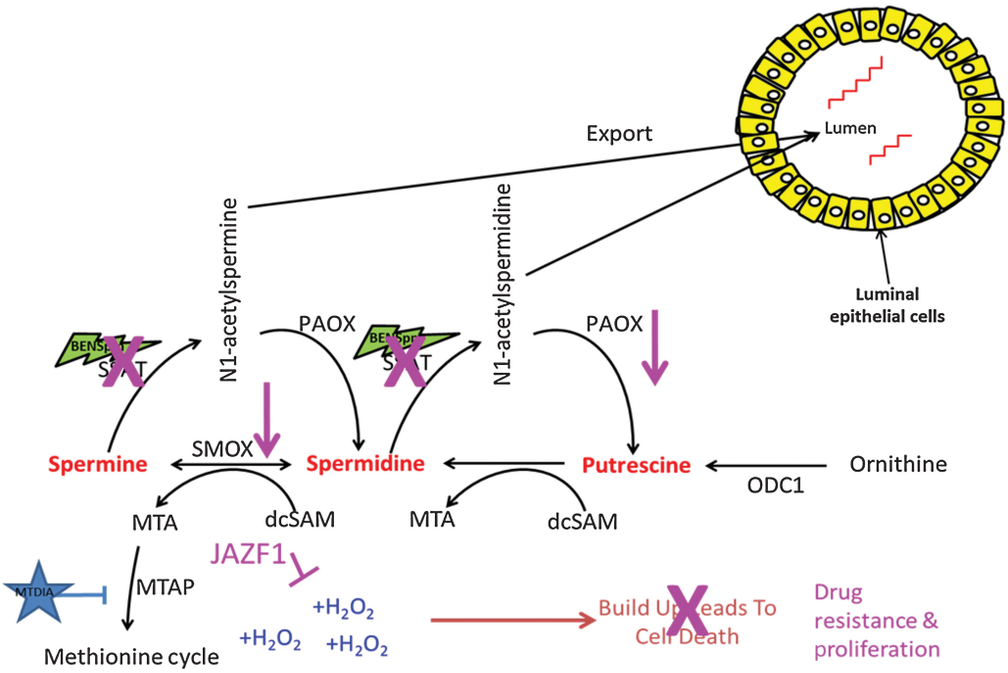

Figure 6.
Proposed effects of JAZF1 on polyamine biosynthesis and combination therapy. JAZF1 decreases the levels of SSAT, and induction of SSAT enzymatic activity induced by BENSpm. It also decreases the transcriptional levels of PAOX and SMOX, the major ROS producers, thereby decreasing both basal ROS accumulation and induction by therapy. This leads to drug resistance and cellular proliferation with therapeutic intervention.

mechanism of action of polyamine-targeted therapies, reduces the efficacy of these drugs.

Most strikingly, *JAZF1* expression is associated with an overall reduction in the expression of polyamine genes and thereby a predicted decreased dependence on this pathway. This, therefore, suggests polyamine-targeted therapies would be less effective in patients that highly express *JAZF1*. TCGA data shows high negative correlation between expression of *JAZF1* and polyamine genes, further strengthening the idea that *JAZF1* may represent a potential biomarker of decreased sensitivity to polyamine-targeted therapies. The overall proposed mechanism of action of these drugs is, therefore, that JAZF1 is reducing the accumulation of ROS by inhibiting the ability of BENSpm to function on SSAT, which is also transcriptionally decreased, leading to cell survival (**Fig. 6**).

This study is limited for a few reasons. Firstly, the use of *JAZF1* as a potential biomarker of response hinges on the utilization of 9 samples. To further confirm these results and ensure the clinical efficacy of *JAZF1* as a biomarker, in regard to polyamine-targeted therapies, more *ex vivo* patient samples would need to be considered. In addition, this study only considered a single combination therapy targeting the polyamine biosynthetic pathway. Specifically, a strategy to increase the stress of high flux through polyamine metabolism by activating catabolism, while simultaneously inhibiting the methionine salvage pathway which helps to relieve metabolic stress from the high flux. Other polyamine-targeted strategies work by inhibiting biosynthesis and uptake of polyamines, such as using the ODC1 inhibitor difluoromethylornithine (DFMO) in combination with the polyamine import blocker polyamine transport inhibitor, AMXT-1501. The observation that high level *JAZF1* leads to reduction in expression of polyamine pathway genes suggest the possibility that those patients with high levels of *JAZF1* might respond better to approaches that aim to starve the cells of polyamine production and import.

Authors' Disclosures

S.R. Rosario reports grants from NIH; and grants from NCI during the conduct of the study. H.C. Affronti reports a patent 11045473 issued. No disclosures were reported by the other authors.

Authors' Contributions

S.R. Rosario: Conceptualization, data curation, software, formal analysis, validation, investigation, visualization, methodology, writing–original draft, writing–review and editing. **J.J. Jacobi:** Formal analysis, validation, investigation, visualization, methodology, writing–review and editing. **M.D. Long:** Conceptualization, formal analysis, supervision, validation, investigation, visualization, methodology, writing–review and editing. **H.C. Affronti:** Formal analysis, validation, writing–review and editing. **A.M. Rowsam:** Conceptualization, validation, investigation, writing–review and editing. **D.J. Smiraglia:** Conceptualization, resources, supervision, funding acquisition, investigation, visualization, methodology, project administration, writing–review and editing.

Acknowledgments

This work was supported in part by the following: NIH R01CA197996 (to D.J. Smiraglia); NIH R01CA197996–02S, R25 CA20365, and U24 CA232979–01S5 (to S.R. Rosario); NIH F99CA21245501 (to H.C. Affronti). NCI grant P30CA016056 involving the use of Roswell Park Cancer Institute's Mouse Tumor Model, Department of Laboratory Animal Research, Genomic, Biostatistics, and Bioanalytics, Metabolomics & Pharmacokinetics Shared Resources; The Roswell Park Alliance Foundation.

The publication costs of this article were defrayed in part by the payment of publication fees. Therefore, and solely to indicate this fact, this article is hereby marked "advertisement" in accordance with 18 USC section 1734.

Note

Supplementary data for this article are available at Molecular Cancer Research Online (http://mcr.aacrjournals.org/).

Received April 15, 2022; revised August 5, 2022; accepted September 22, 2022; published first September 27, 2022.

References

1. Sullivan DM, Chow KC, Glisson BS, Ross WE. Role of proliferation in determining sensitivity to topoisomerase II–active chemotherapy agents. NCI Monogr 1987:73–8.
2. Klein HO, Gross R. Experimental and clinical results of chemotherapy after partial synchronization of cell proliferation. Recent Results Cancer Res 1975:215–24.
3. Dobashi Y, Goto A, Endo T, Ooi A. Genetic aberrations as the targets of oncology research: Involvement of paraffin-embedded tissues. Histol Histopathol 2014;29: 191–205.
4. Kim SY, Kim SM, Chang H, Kim BW, Lee YS, Chang HS, et al. Safety of tyrosine kinase inhibitors in patients with differentiated thyroid cancer: real-world use of lenvatinib and sorafenib in Korea. Front Endocrinol 2019;10:384.
5. Li J, Halfter K, Zhang M, Saad C, Xu K, Bauer B, et al. Computational analysis of receptor tyrosine kinase inhibitors and cancer metabolism: implications for treatment and discovery of potential therapeutic signatures. BMC Cancer 2019; 19:600.
6. Gonzalez-Martin A, Sanchez-Lorenzo L. Immunotherapy with checkpoint inhibitors in patients with ovarian cancer: still promising? Cancer 2019;125: 4616–22.
7. Duan J, Cui L, Zhao X, Bai H, Cai S, Wang G, et al. Use of immunotherapy with programmed cell death 1 versus programmed cell death ligand 1 inhibitors in patients with cancer: a systematic review and meta-analysis. JAMA Oncol 2020; 6:375–84.
8. Vander Heiden MG, Cantley LC, Thompson CB. Understanding the Warburg effect: the metabolic requirements of cell proliferation. Science 2009; 324:1029–33.
9. Jones RG, Thompson CB. Tumor suppressors and cell metabolism: a recipe for cancer growth. Genes Dev 2009;23:537–48.
10. Choi YK, Park KG. Targeting glutamine metabolism for cancer treatment. Biomol Ther 2018;26:19–28.
11. Luengo A, Gui DY, Vander Heiden MG. Targeting metabolism for cancer therapy. Cell Chem Biol 2017;24:1161–80.
12. Pacheco MP, Bintener T, Ternes D, Kulms D, Haan S, Letellier E, et al. Identifying and targeting cancer-specific metabolism with network-based drug target prediction. EBioMedicine 2019;43:98–106.
13. Weiss JM. The promise and peril of targeting cell metabolism for cancer therapy. Cancer Immunol Immunother 2020;69:255–61.
14. Rosario SR, Long MD, Affronti HC, Rowsam AM, Eng KH, Smiraglia DJ. Pancancer analysis of transcriptional metabolic dysregulation using The Cancer Genome Atlas. Nat Commun 2018;9:5330.
15. Affronti HC, Rowsam AM, Pellerite AJ, Rosario SR, Long MD, Jacobi JJ, et al. Pharmacological polyamine catabolism upregulation with methionine salvage pathway inhibition as an effective prostate cancer therapy. Nat Commun 2020; 11:52.
16. Seo MK, Cairns J. Do cancer biomarkers make targeted therapies cost-effective? A systematic review in metastatic colorectal cancer. PLoS One 2018;13:e0204496.
17. Liao ZZ, Wang YD, Qi XY, Xiao XH. JAZF1, a relevant metabolic regulator in type 2 diabetes. Diabetes Metab Res Rev 2019;35:e3148.
18. Langberg KA, Ma L, Sharma NK, Hanis CL, Elbein SC, Hasstedt SJ, et al. Single-nucleotide polymorphisms in JAZF1 and BCL11A gene are nominally associated with type 2 diabetes in African-American families from the GENNID study. J Hum Genet 2012;57:57–61.
19. Stevens VL, Ahn J, Sun J, Jacobs EJ, Moore SC, Patel AV, et al. HNF1B and JAZF1 genes, diabetes, and prostate cancer risk. Prostate 2010;70:601–7.
20. Hu WJ, Shen WW, Li XJ, Yao J, Jia YJ, Fan XY. [Effect of JAZF1 overexpression on high-fat diet-induced nonalcoholic fatty liver disease]. Zhonghua Gan Zang Bing Za Zhi 2016;24:596–600.
21. Wei Q, Zhou B, Yang G, Hu W, Zhang L, Liu R, et al. JAZF1 ameliorates age and diet-associated hepatic steatosis through SREBP-1c–dependent mechanism. Cell Death Dis 2018;9:859.
22. Jang WY, Bae KB, Kim SH, Yu DH, Kim HJ, Ji YR, et al. Overexpression of Jazf1 reduces body weight gain and regulates lipid metabolism in high fat diet. Biochem Biophys Res Commun 2014;444:296–301.
23. Li L, Yang Y, Yang G, Lu C, Yang M, Liu H, et al. The role of JAZF1 on lipid metabolism and related genes in vitro. Metabolism 2011;60:523–30.
24. Ma X, Wang J, Wang J, Ma CX, Gao X, Patriub V, et al. The JAZF1-SUZ12 fusion protein disrupts PRC2 complexes and impairs chromatin repression during human endometrial stromal tumorogenesis. Oncotarget 2017;8:4062–78.
25. Panagopoulos I, Mertens F, Griffin CA. An endometrial stromal sarcoma cell line with the JAZF1/PHF1 chimera. Cancer Genet Cytogenet 2008;185:74–7.
26. Sung Y, Park S, Park SJ, Jeong J, Choi M, Lee J, et al. Jazf1 promotes prostate cancer progression by activating JNK/Slug. Oncotarget 2018;9:755–65.
27. Wang KS, Zuo L, Owusu D, Pan Y, Luo X. Prostate cancer related JAZF1 gene is associated with Schizophrenia. J Schizophr Res 2014;1:1002.
28. Prokunina-Olsson L, Fu YP, Tang W, Jacobs KB, Hayes RB, Kraft P, et al. Refining the prostate cancer genetic association within the JAZF1 gene on chromosome 7p15.2. Cancer Epidemiol Biomarkers Prev 2010;19:1349–55.
29. Li Y, Kang K, Krahn JM, Croutwater N, Lee K, Umbach DM, et al. A comprehensive genomic pan-cancer classification using The Cancer Genome Atlas gene expression data. BMC Genomics 2017;18:508.
30. Taylor BS, Schultz N, Hieronymus H, Gopalan A, Xiao Y, Carver BS, et al. Integrative genomic profiling of human prostate cancer. Cancer Cell 2010;18: 11–22.
31. Bistulfi G, Diegelman P, Foster BA, Kramer DL, Porter CW, Smiraglia DJ. Polyamine biosynthesis impacts cellular folate requirements necessary to maintain S-adenosylmethionine and nucleotide pools. FASEB J 2009;23:2888–97.
32. Seedhouse SJ, Affronti HC, Karasik E, Gillard BM, Azabdaftari G, Smiraglia DJ, et al. Metastatic phenotype in CWR22 prostate cancer xenograft following castration. Prostate 2016;76:359–68.
33. Ritchie ME, Phipson B, Wu D, Hu Y, Law CW, Shi W, et al. limma powers differential expression analyses for RNA sequencing and microarray studies. Nucleic Acids Res 2015;43:e47.
34. Pang Z, Chong J, Zhou G, de Lima Morais DA, Chang L, Barrette M, et al. MetaboAnalyst 5.0: narrowing the gap between raw spectra and functional insights. Nucleic Acids Res 2021;49:W388–96.
35. Soneson C, Love MI, Robinson MD. Differential analyses for RNA-seq: transcript-level estimates improve gene-level inferences. F1000Res 2015;4: 1521.
36. Shannon P, Markiel A, Ozier O, Baliga NS, Wang JT, Ramage D, et al. Cytoscape: a software environment for integrated models of biomolecular interaction networks. Genome Res 2003;13:2498–504.
37. Ogata H, Goto S, Sato K, Fujibuchi W, Bono H, Kanehisa M. KEGG: Kyoto encyclopedia of genes and genomes. Nucleic Acids Res 1999;27:29–34.
38. Janky R, Verfaillie A, Imrichova H, Van de Sande B, Standaert L, Christiaens V, et al. iRegulon: from a gene list to a gene regulatory network using large motif and track collections. PLoS Comput Biol 2014;10:e1003731.
39. Burgess SJ, Reyna-Llorens I, Stevenson SR, Singh P, Jaeger K, Hibberd JM. Genome-wide transcription factor binding in leaves from C3 and C4 grasses. Plant Cell 2019;31:2297–314.
40. Oesper L, Merico D, Isserlin R, Bader GD. WordCloud: a Cytoscape plugin to create a visual semantic summary of networks. Source Code Biol Med 2011;6:7.
41. Bang LG, Dasari VR, Kim D, Gogoi RP. Differential gene expression induced by verteporfin in endometrial cancer cells. Sci Rep 2019;9:3839.
42. Maag JLV. gganatogram: an R package for modular visualisation of anatograms and tissues based on ggplot2. F1000Res 2018;7:1576.
43. Ito K, Murphy D. Application of ggplot2 to pharmacometric graphics. CPT Pharmacometrics Syst Pharmacol 2013;2:e79.
44. Bianchi-Smiraglia A, Bagati A, Fink EE, Affronti HC, Lipchick BC, Moparthy S, et al. Inhibition of the aryl hydrocarbon receptor/polyamine biosynthesis axis suppresses multiple myeloma. J Clin Invest 2018;128:4682–96.
45. Grivennikova VG, Kareyeva AV, Vinogradov AD. Oxygen-dependence of mitochondrial ROS production as detected by Amplex Red assay. Redox Biol 2018;17:192–9.
46. Lee CW, Chen YC, Ostafin A. The accuracy of Amplex Red assay for hydrogen peroxide in the presence of nanoparticles. J Biomed Nanotechnol 2009;5:477–85.
47. Casero RA Jr, Celano P, Ervin SJ, Wiest L, Pegg AE. High specific induction of spermidine/spermine N1-acetyltransferase in a human large cell lung carcinoma. Biochem J 1990;270:615–20.
48. Casero RA Jr, Celano P, Ervin SJ, Porter CW, Bergeron RJ, Libby PR. Differential induction of spermidine/spermine N1-acetyltransferase in human lung cancer cells by the bis(ethyl)polyamine analogues. Cancer Res 1989;49:3829–33.
49. Franken NA, Rodermond HM, Stap J, Haveman J, van Bree C. Clonogenic assay of cells in vitro. Nat Protoc 2006;1:2315–9.
50. Wu WY, Morris RJ. Method for the harvest and assay of in vitro clonogenic keratinocytes stem cells from mice. Methods Mol Biol 2005;289:79–86.